Electronic Supplementary Material (ESI) for Inorganic Chemistry Frontiers.

Supporting Information

Designing heterostructurated core@satellites Prussian Blue Analogue@Au-Ag nanoparticles: effect on the magnetic properties and catalytic activity

Ekaterina Mamontova,[a] María Rodríguez-Castillo,[b] Erwan Oliviero,[a,c] Yannick Guari,[a] Joulia Larionova*[a], Miguel Monge*[b] and Jérôme Long*[a]

a. ICGM, Univ. Montpellier, CNRS, ENSCM, Montpellier, France.

b. Departamento de Química, Universidad de La Rioja, Centro de Investigación en Síntesis Química (CISQ), Complejo Científico-Tecnológico, 26004, Logroño, Spain.

c. MEA Plateform, Université de Montpellier, Montpellier, France.

Table of Contents

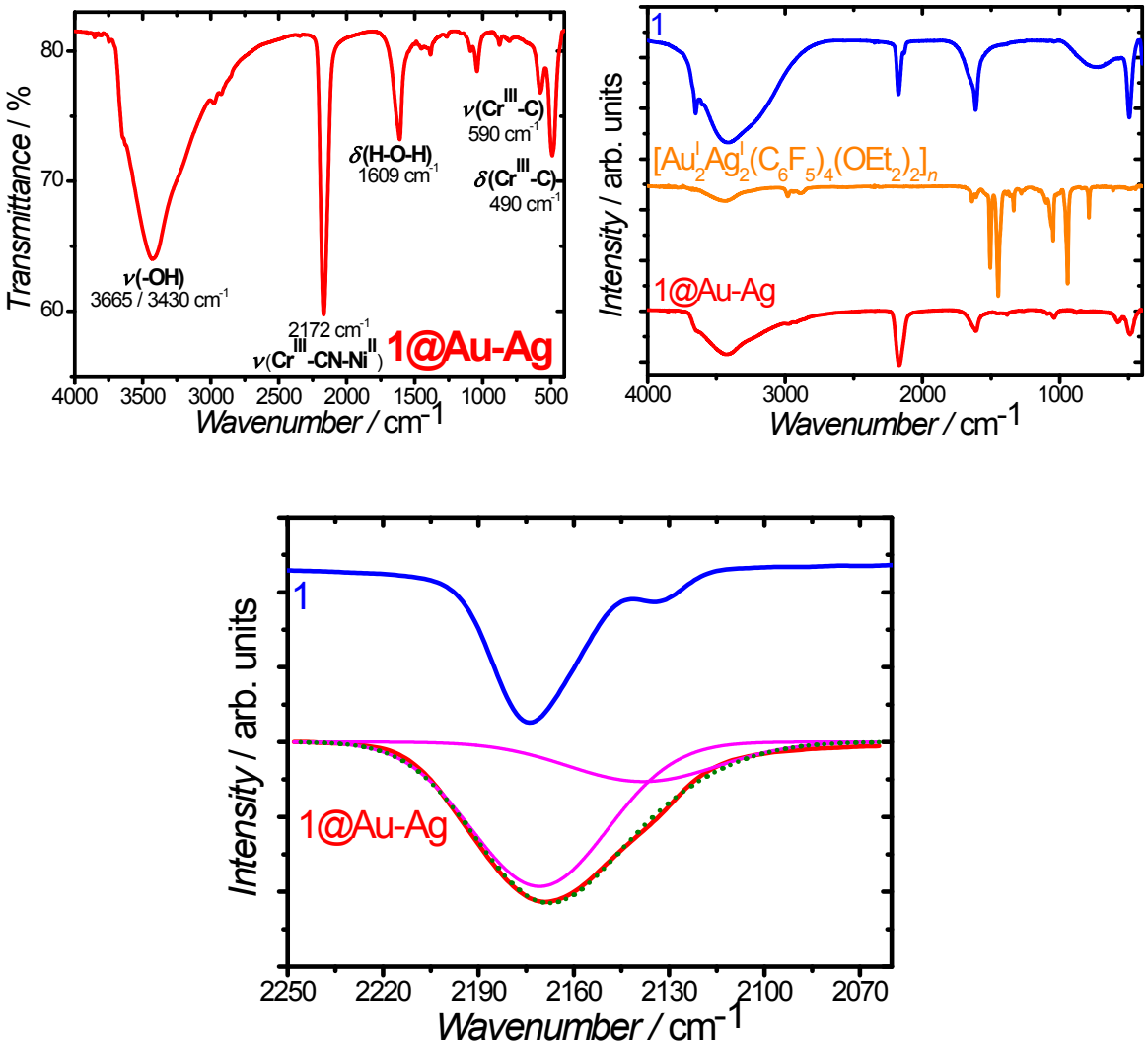

Fig. S1. IR spectra of **1@Au-Ag** (Top, Left) and comparison between IR spectra of **1**, Au-Ag precursor and **1@Au-Ag** (Top, Right). Bottom: magnification in the cyanide region. The two deconvoluted peaks are shown in purple whereas the cumulative fit appears as a dot green line.

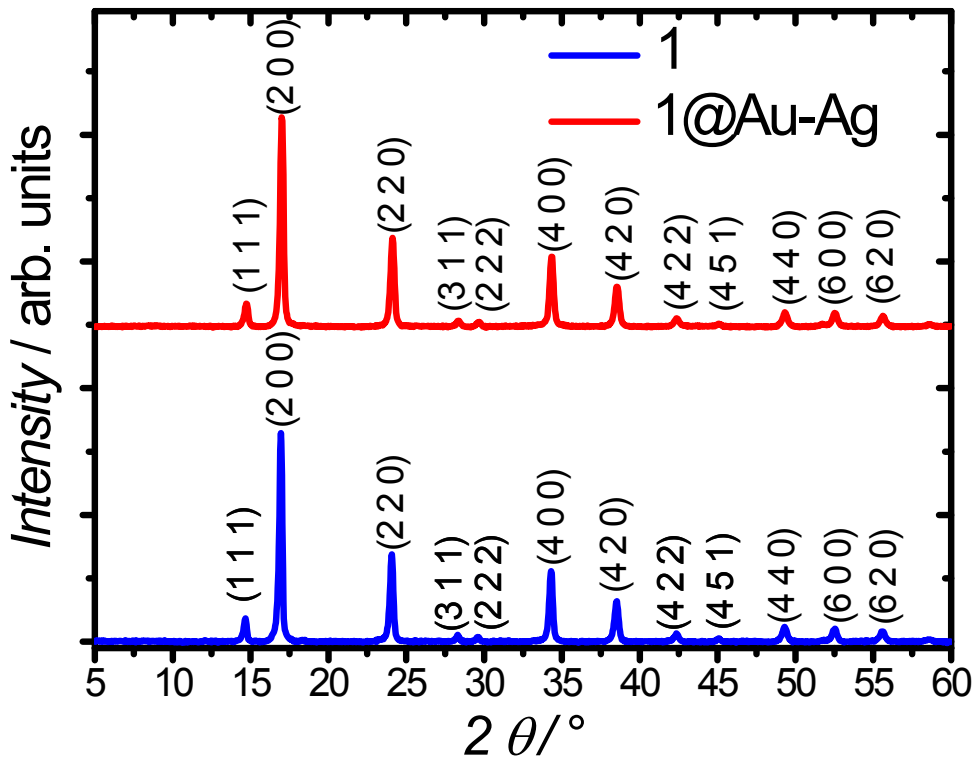

Fig. S2. PXRD patterns of **1** and **1@Au-Ag**.

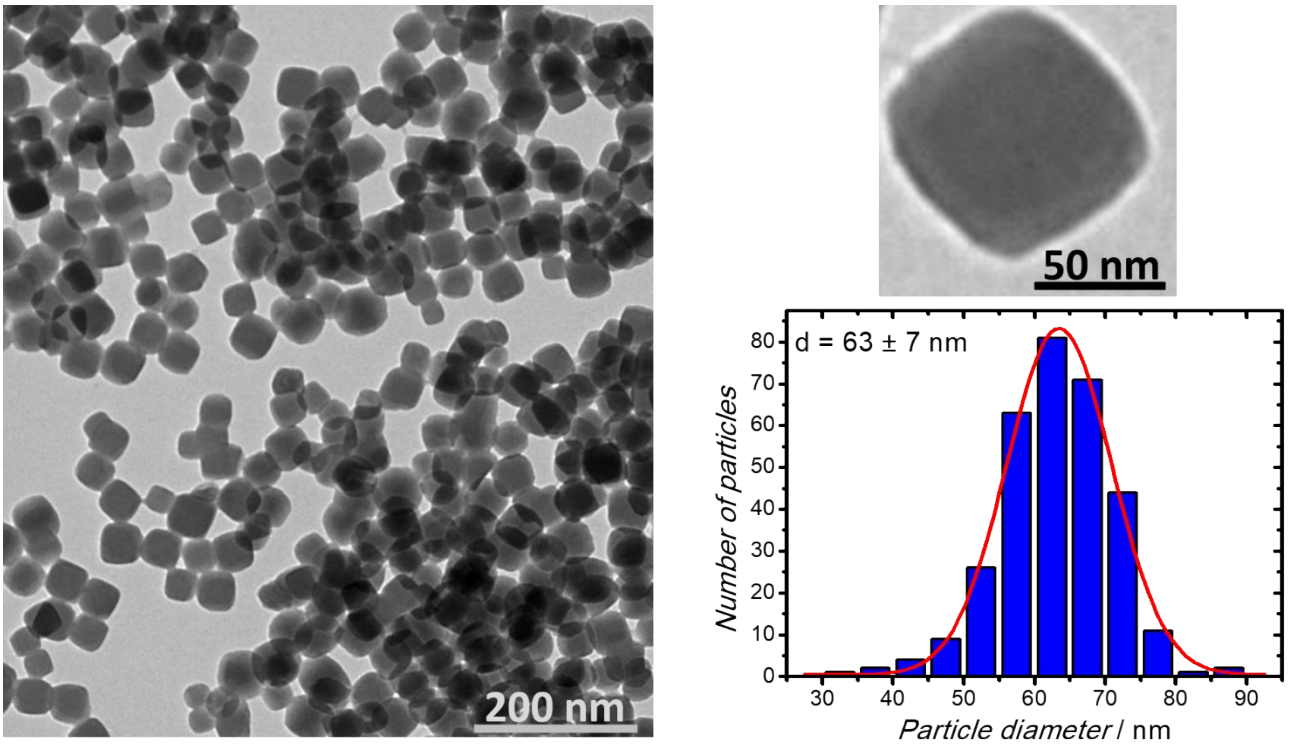

Fig. S3. TEM image and size distribution for **1**.

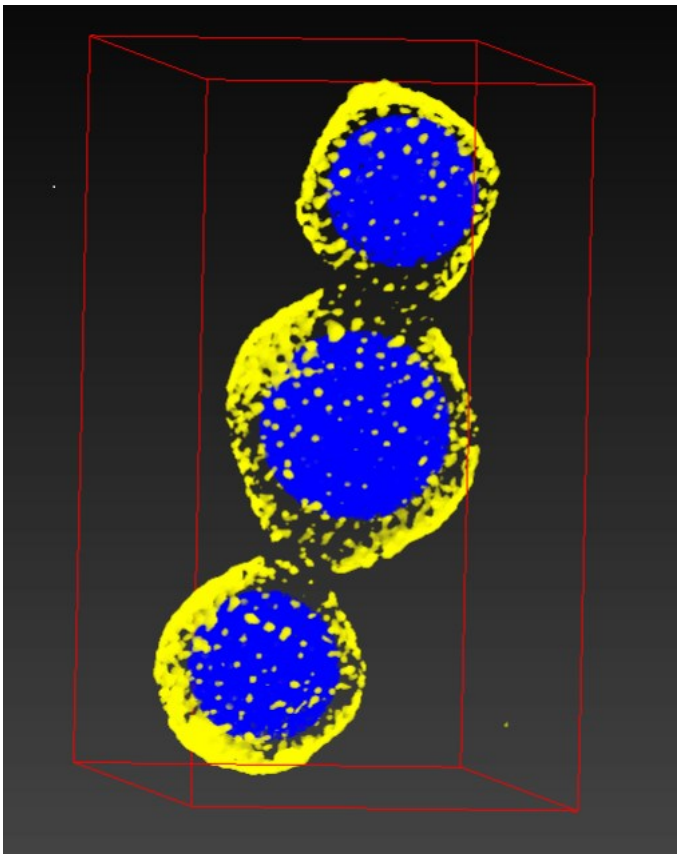

Fig. S4. 3D TEM reconstruction for **1@Au-Ag**.

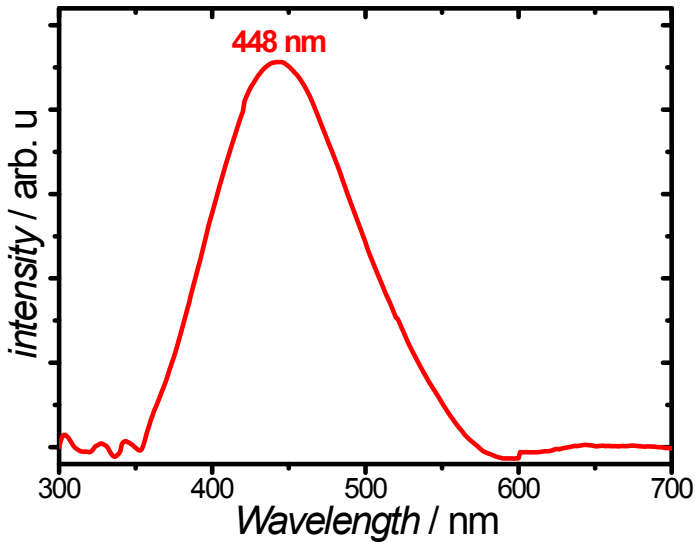

Fig. S5. Estimation of the SPR maximum wavelength for **1@Au-Ag** by taking into account the NiCr PBA contribution to the electronic spectrum.

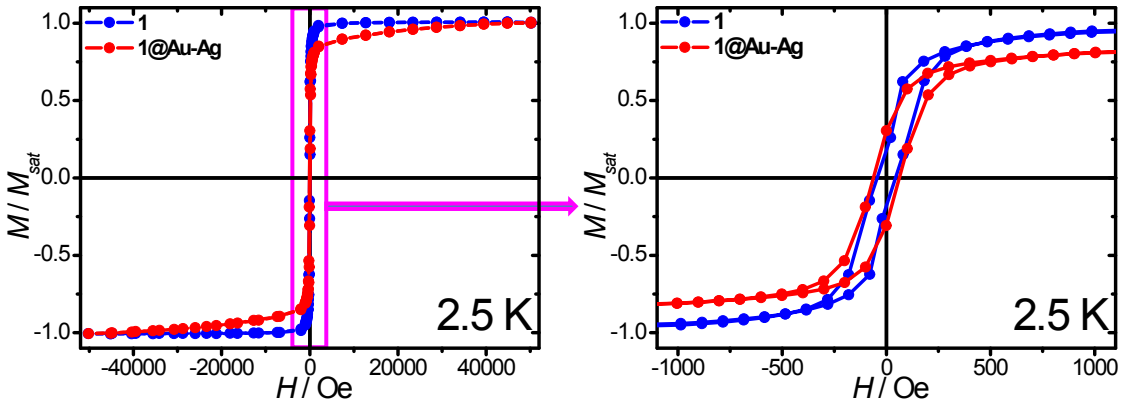

Fig. S6. Hysteresis loops for **1** and **1@Au-Ag** at 2.5 K. For comparison, the data have been normalized with the values measured at 50 kOe (M_{sat}).

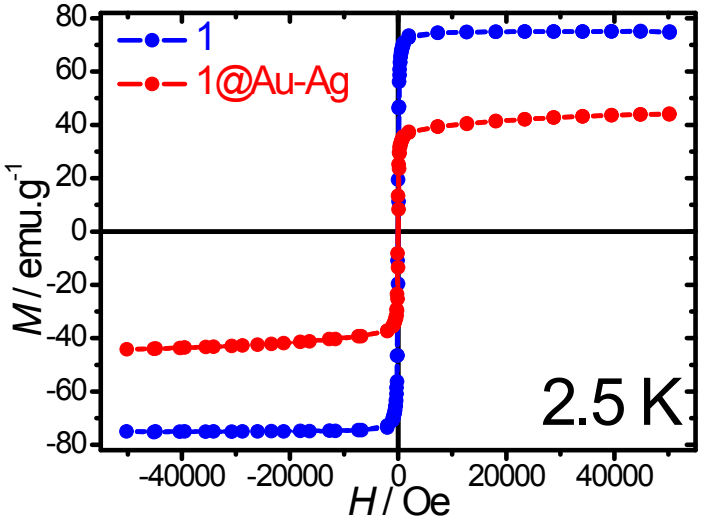

Fig. S7. Hysteresis loops for **1** and **1@Au-Ag** at 2.5 K expressed as emu.g^{-1}.

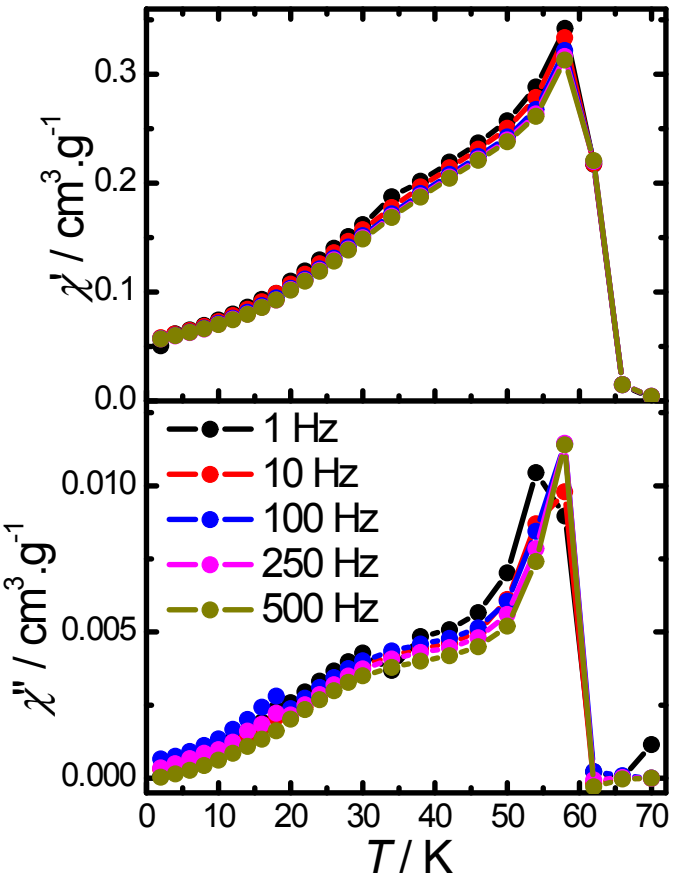

Fig. S8. Temperature dependence of the in-phase (χ') and out-of-phase (χ'') susceptibility components for **1**.

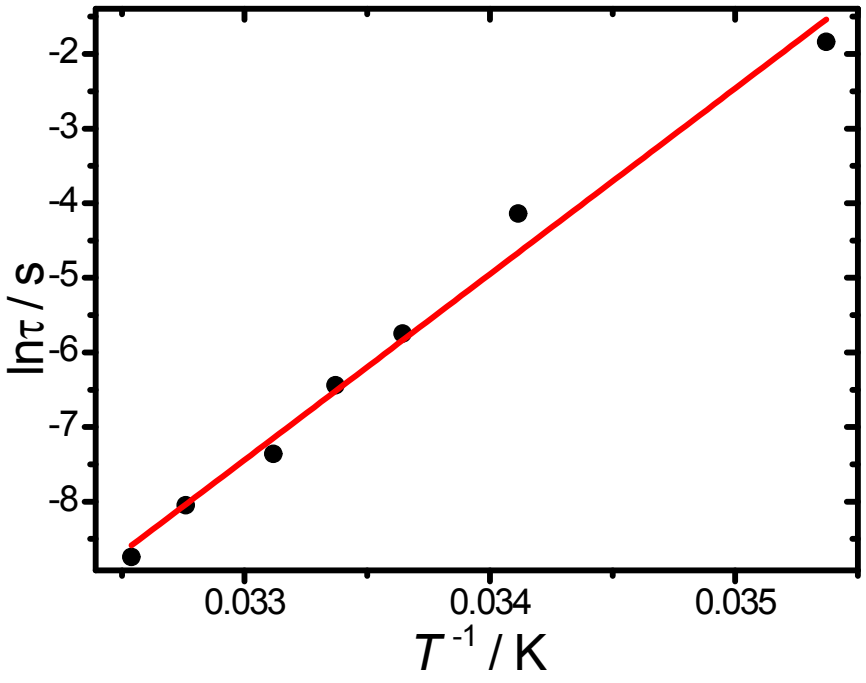

Fig. S9. Temperature dependence of the relaxation time for **1@Au-Ag**. The red line represents the fit with an Arrhenius law.

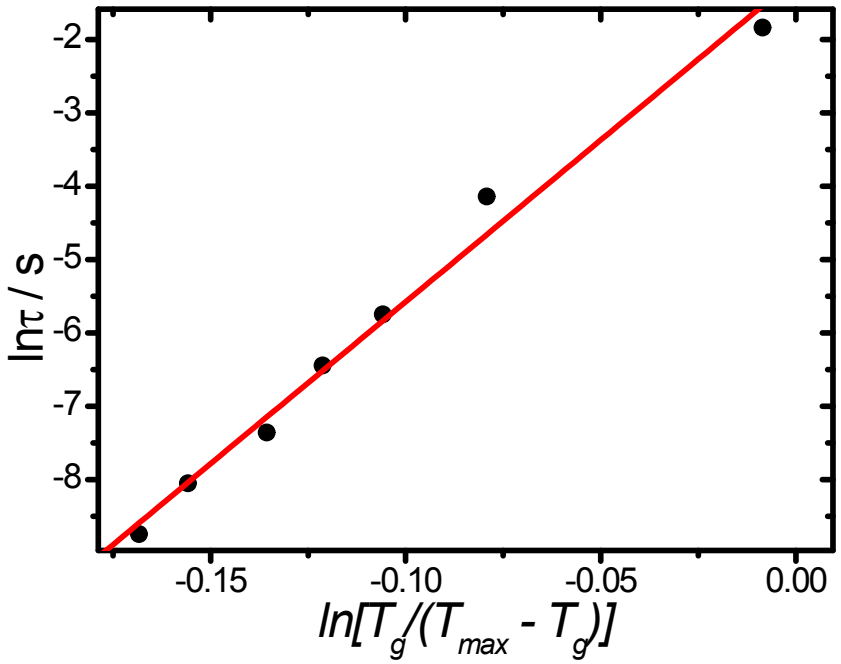

Fig. S10. Critical scaling law fitting for **1@Au-Ag.**

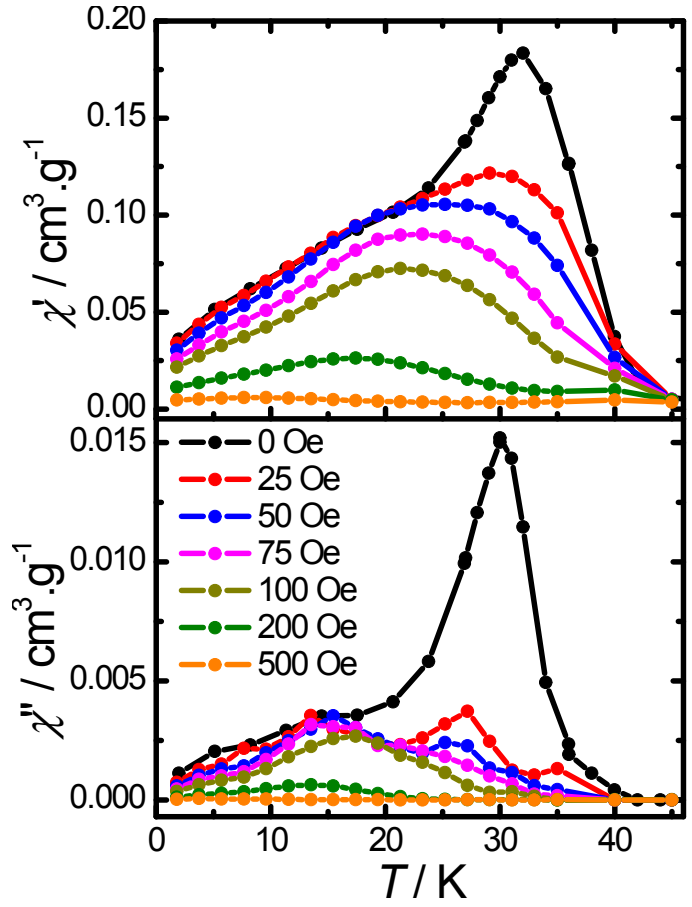

Fig. S11. Temperature dependence of the in-phase (χ') and out-of-phase (χ") susceptibility components at 100 Hz at various dc fields for **1@Au-Ag**.

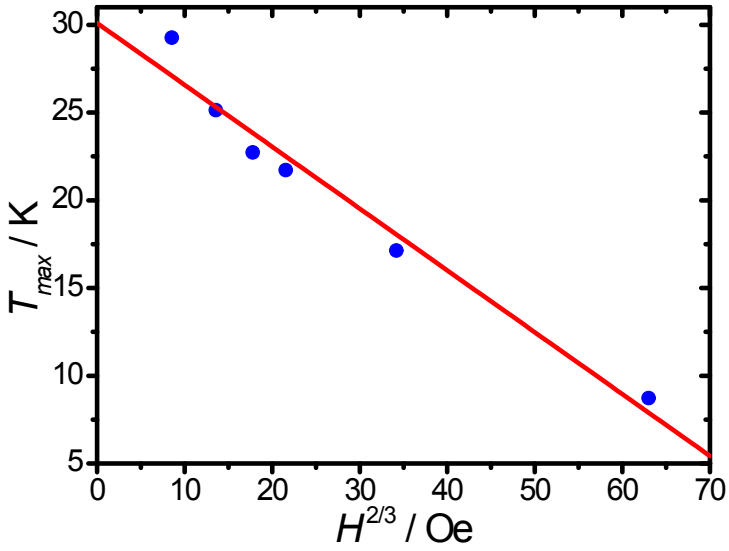

Fig. S12. Field dependence of the temperature maximum of χ'' as a function of the magnetic field (Almeida–Thouless line) for for **1@Au-Ag**.

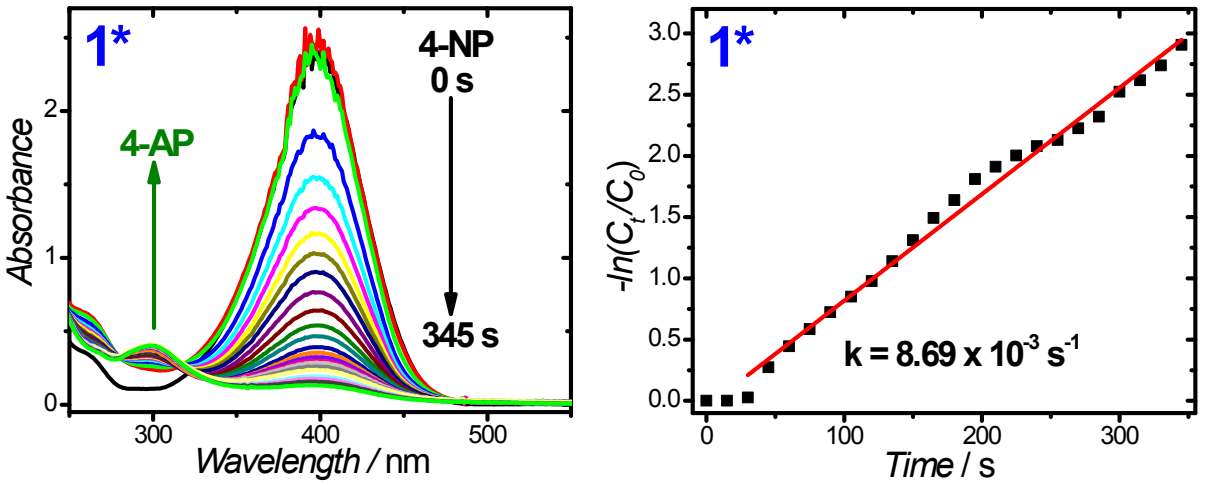

Fig S13. (Left) Time-dependent UV-Vis absorption spectra of 4-NP (400 nm) and 4-AP (295 nm) during reduction catalysed by **1*** (* = in the experimental conditions reported by Lin and co-workers[1]); (Right) Plot of $-ln(C_t/C_0)$ as a function of time for reaction catalysed by **1***.

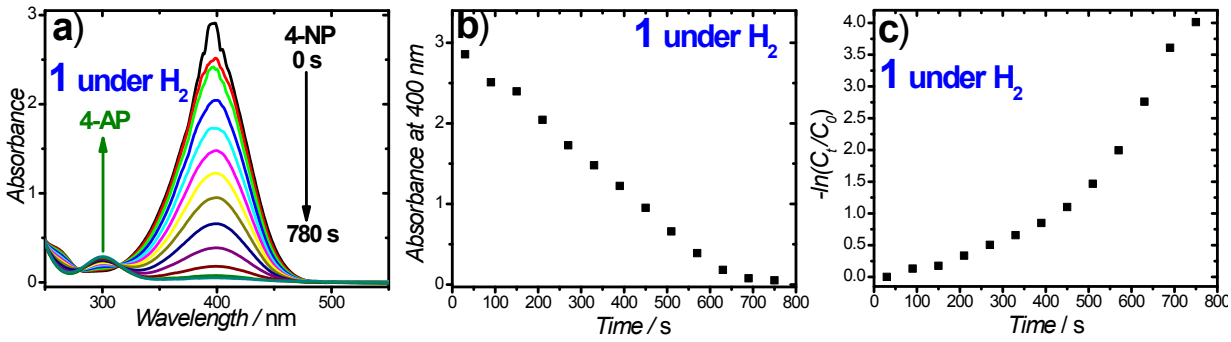

Fig S14. a) Time-dependent UV-Vis absorption spectra of 4-NP (400 nm) and 4-AP (295 nm) during reduction catalysed by **1** under H_2. b) Plot of the absorbance at 400 nm as a function of time. C) Plot of $-ln(C_t/C_0)$ as a function of time for reaction catalysed by **1** under H_2.

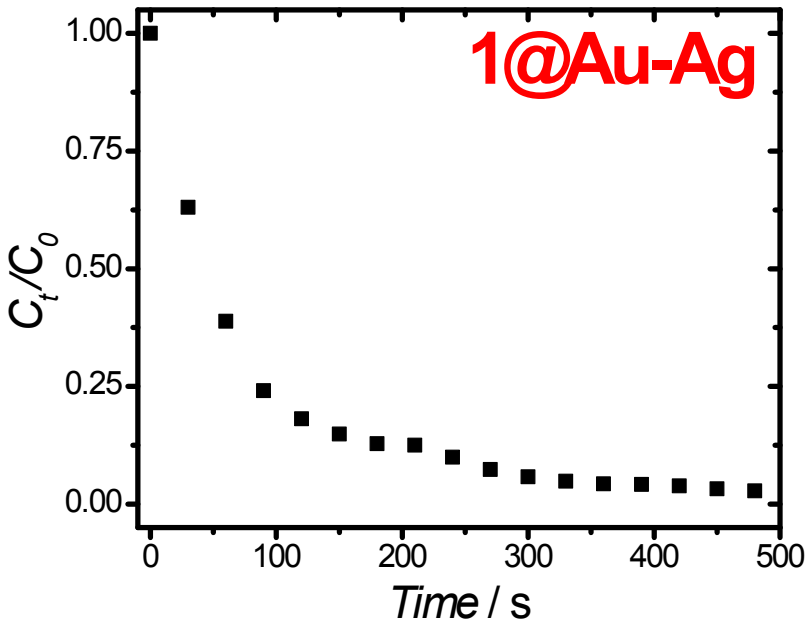

Fig S15. Plot of C_t/C_0 as a function of time for reaction catalysed by **1@Au-Ag.**

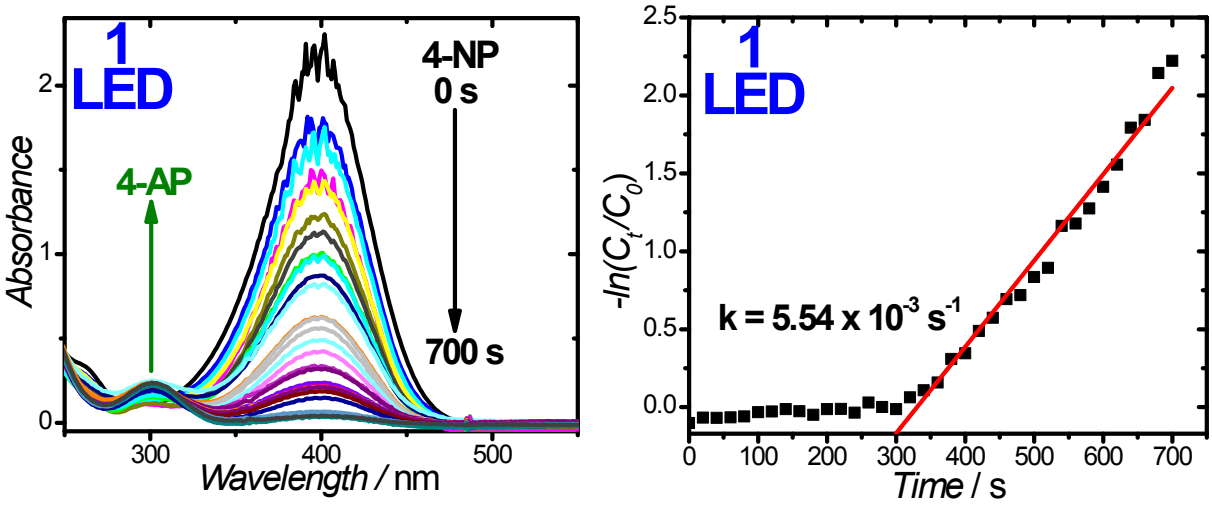

Fig S16. (Left) Time-dependent UV-Vis absorption spectra of 4-NP (400 nm) and 4-AP (295 nm) during reduction catalysed by **1** under LED light irradiation; (Right) Plot of $-ln(C_t/C_0)$ as a function of time for reaction catalysed by **1** under LED light irradiation.

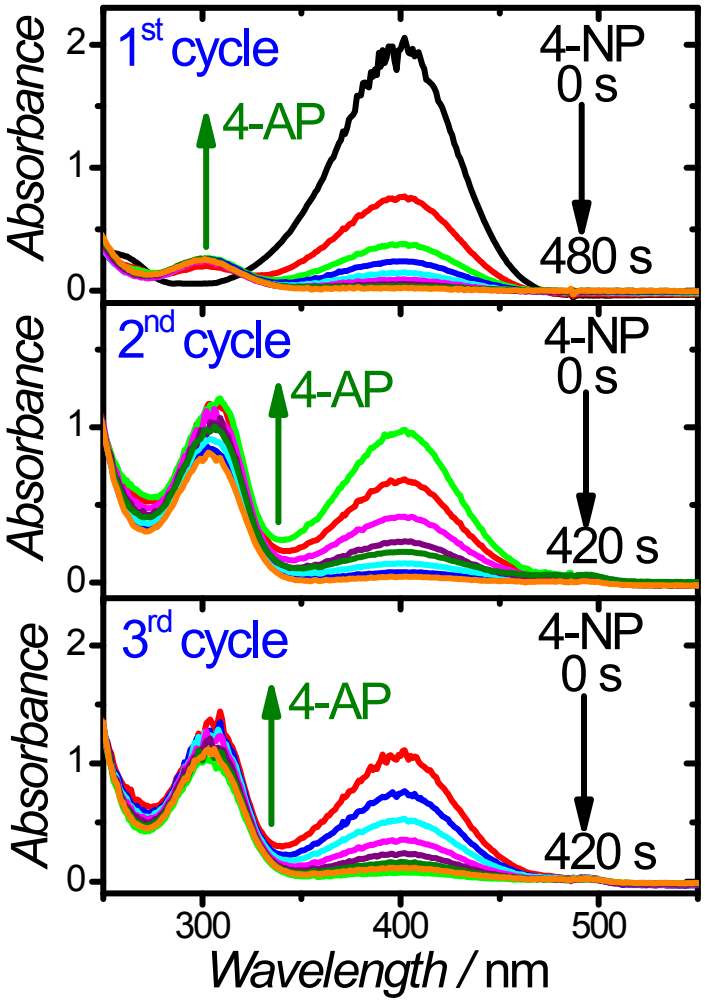

Fig S17. Time-dependent UV-Vis absorption spectrum of the reduction of 4-NP (400 nm) and the formation of 4-AP (295 nm) measured for three reaction cycles illustrating the reusability of catalyst **1@Au-Ag**.

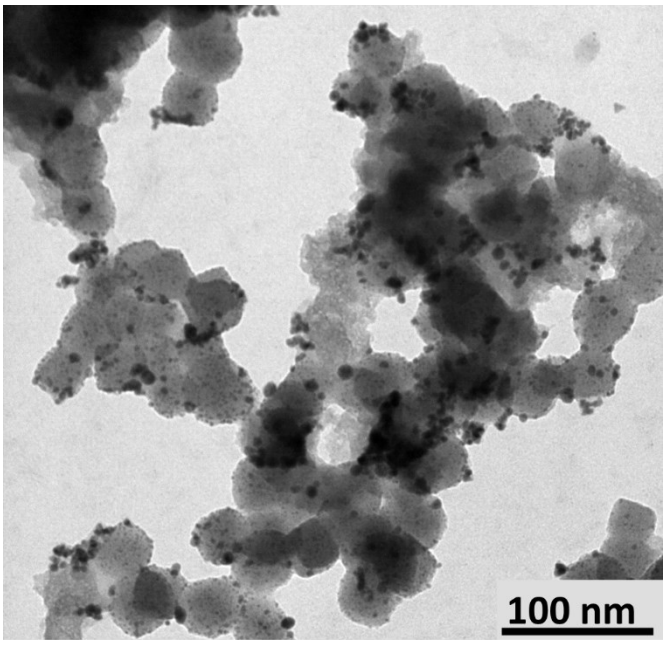

Fig S18. TEM image of **1@Au-Ag** after the first catalytic cycle of reduction of 4-NP, showing that the morphology of the nanostructure is preserved after catalysis.

References

1 T. Wi-Afedzi, F.-Y. Yeoh, M.-T. Yang, A. C. K. Yip and K.-Y. A. Lin, *Sep. Purif. Technol.*, 2019, **218**, 138-145.